2023

# The Encapsulation of Enzymes in Multiphase Complex Coacervates

Akash R. Rajaram
*University of Central Florida*

# THE ENCAPSULATION OF ENZYMES IN MULTIPHASE COMPLEX COACERVATES

by

AKASH RAJARAM

A thesis submitted in partial fulfillment of the requirements for
the Honors in the Major Program in Biomedical Sciences
in the College of Medicine
and in the Burnett Honors College
at the University of Central Florida
Orlando, Florida

Spring Term, 2023

Thesis Chair: Lorraine Leon, Ph.D.

# ABSTRACT

Polyelectrolyte complex coacervates (PECCs) result from liquid-liquid phase separation (LLPS) in solutions containing oppositely charged polymers [1]. Multiphase polyelectrolyte complex coacervates (MPECCs) result from the combination of multiple, specific PECCs [2]. The encapsulation of proteins in PECCs can serve as promising vehicles for the effective delivery of protein-based therapeutics, which are notoriously difficult to deliver. The encapsulation of model proteins, such as Bovine Serum Albumin (BSA) [3] or Human Hemoglobin (Hb) [4] have illustrated the protein-encapsulating capabilities of these PECC systems. The encapsulation of proteins in MPECCs is a topic that has yet to be explored; however, it can serve to mimic the structure and function of multiphase membraneless organelles, which are abundantly available in cells. This project sought to understand and quantify the encapsulation of enzymes in both PECC and MPECC models; as well as evaluate their efficiency upon encapsulation, as enzymes are simply proteins with catalytic functions [5]. A synthesized library of charged, heterochiral polypeptides were used to form both PECC and MPECC systems. Glucose oxidase (GOx) and horseradish peroxidase (HRP) were the enzymes chosen to be assessed in both PECC and MPECC systems. Turbidity measurements, in terms of percent mole of polycation, were used to determine the optimal stoichiometric ratio between the polyanion and polyanion, in the presence of a given concentration of both or either enzyme, in which maximum complex formation occurred. Here we report that a 1:1 stoichiometric ratio of polycation to polyanion in either a solution with 25ug/mL HRP and 25ug/mL GOx, a solution with 50ug/mL GOx, or a solution with 50ug/mL HRP leads to the highest level of complexation. Enzyme encapsulation efficiency of individual PECCs for both enzymes was assessed using the Bradford assay, in which the supernatant was used to determine the concentration of enzyme left in the PECC post-centrifugation. Here we

report that all PECC systems were able to encapsulate both GOx and HRP. Higher encapsulation efficiencies were seen with GOx samples compared to HRP samples. Enzymatic activity and efficiency were assessed using the 2,2'-azino-bis(3-ethylbenzothiazoline-6-sulfonic acid (ABTS) assay in the presence of ß-D-glucose. The chromogenic change in intensity over time of each sample was assessed using optical microscopy. Michaelis-Menten graphs were made from the data collected. The resulting data was used to evaluate the $K_m$ and $V_{max}$ of the enzyme cascade in PECC and MPECC systems compared to a control. Here we report that enzyme cascade efficiency varied among PECC and MPECC samples, with some being more efficient than others. We find that both PECC and MPECC systems generally have lower enzyme-substrate affinity (higher $K_m$) compared to performing the reactions in water. However, this may be related to the need for the substrate to diffuse into a different phase or phases. Interestingly, many of the PECC and MPECC systems have lower $V_{max}$ values compared to the water control, indicating a faster enzyme saturation. The enzyme kinetics and efficiency could also be controlled by varying the location of the enzymes in each phase within the MPECC systems. Overall, we show that using MPECC systems allows one to select advantageous properties of individual PECCs and combine them together.

# ACKNOWLEDGEMENTS

I am thankful for the myriad of individuals who have aided in the conceptualization of this thesis. Multiple members of the Biomolecular Engineering Laboratory, led by Dr. Lorraine Leon, have helped with the collection and analysis of data. Thank you Dr. Sara Tabandeh, Ph.D, for formulating the charged polypeptides used in this thesis and getting me started with this project to begin with. Thank you Tahoora Ateeq, for helping me develop protocols and analyze data, even when it seemed indecipherable. Thank you to Lindsey Rush, for carrying out experiments and formulating stock solutions for this project.

Thank you to my parents, Nadia and Parsram Rajaram, and my sisters, Sanjana and Shweta Rajaram, for their continuous love and support throughout my entire undergraduate research career. Thank you to my grandparents, Latchmin and Lackrajh Mattai, for always being there when I needed advice the most. Thank you to the Payman and Maragh families, for always cheering me on as I progress through my academics. Thank you to my late great-grandmother, Ratni Singh, for your continuous encouragement and blessings.

Thank you to my significant other, Krupa Patel, for always being in my corner. I appreciate all you have done for me. From the proofreading of drafts to the random speeches that boost my motivation, I sincerely appreciate all you do. You have made the late nights and early mornings easier to power on through.

I would like to acknowledge the University of Central Florida's College of Medicine, Burnett Honors College, and the Department of Material Sciences and Engineering for allowing me to conduct my research at their facilities. Thank you to the National Science Foundation, College of Engineering and Computer Science, and the Office of Undergraduate Research for the financial support provided to me.

I would like to give a sincere thank you to my Thesis Chair, Dr. Lorraine Leon, for her continuous support and motivation throughout this project. Thank you for allowing me to independently pursue my work, while also providing me with meaningful advice as a mentor. To my Thesis Committee member, Dr. Kausik Mukhopadhyay, thank you for always being readily available to provide your expertise.

Upon graduating in the Spring term of 2023, I look forward to honing and distributing my research skills and scientific discoveries as a future Ph.D. student.

# TABLE OF CONTENTS

ABSTRACT ..... ii

ACKNOWLEDGEMENTS ..... iv

LIST OF FIGURES ..... vii

LIST OF TABLES ..... ix

LIST OF ABBREVIATIONS ..... x

LIST OF EQUATIONS ..... xi

CHAPTER 1: INTRODUCTION ..... 1

CHAPTER 2: LITERATURE REVIEW ..... 3

2.1: Polyelectrolyte Complex Coacervates ..... 3

2.2: Multiphase Polyelectrolyte Complex Coacervates ..... 7

2.3: Encapsulation of Proteins/Enzymes ..... 9

CHAPTER 3: EXPERIMENTAL METHODOLOGY ..... 12

3.1: Peptide-based PECC Stock Solutions ..... 12

3.2: Enzyme Stock Solutions ..... 12

3.3: Turbidity Test ..... 12

3.4: Enzyme Encapsulation Efficiency ..... 14

3.5 Enzyme Cascade Activity and Efficiency ..... 15

CHAPTER 4: RESULTS AND DISCUSSION ..... 19

4.1: Optical Microscopy of PECC and MPECC Systems ..... 19

4.2: Degree of Turbidity as a Function of Percent mole Polycation ..... 20

4.3: Encapsulation Efficiency of Enzymes by PECCs ..... 23

4.4: Enzyme Cascade Activity and Efficiency in PECC Systems ..... 24

4.5: Enzyme Cascade Activity and Efficiency in MPECC Systems ..... 27

CHAPTER 5: CONCLUSION ..... 30

CHAPTER 6: FURTHER STUDIES ..... 32

REFERENCES ..... 33

# LIST OF FIGURES

Figure 1: Illustration of both liquid-liquid phase separation (right) and liquid-solid phase separation (left). Reproduced from Marciel et al. with permission from Elsevier [16].....3

Figure 2: Image of p(kKa)+p(eEa) in 40mM NaCl. Reproduced from Tabandeh et al. with permission from Molecules [19].....6

Figure 3: Images of multiphase complex coacervates formed via mixing various polymeric complex coacervates. Reproduced from Tiemei et al. from the Journal of the American Chemical Society [2].....8

Figure 4: Schematic of the nucleolus illustrated as a multiphase complex coacervate. Reproduced from Lafontaine et al. with permission from Nature Reviews Molecular Cell Biology [46]. .....9

Figure 5: Encapsulation of glucose oxidase and insulin in a pH-sensitive complex coacervate. Reprinted from Lim et al. with permission from Bioconjugate Chemistry [41].....10

Figure 6: The GOx-HRP enzyme cascade and its quantification using ABTS. Reproduced from Zhang et al. with permission from Nature Communications [53].....11

Figure 7: Enzyme cascade activity and efficiency schematic for MPECC samples.....16

Figure 8: Michaelis-Menten kinetics graphical representation. The initial velocity ($v_0$) is plotted against substrate concentration ([S]). $V_{max}$ and $K_m$ can be calculated from the graph. Reproduced from Wang et al. with permission from Frontiers [57].....17

Figure 9: Images of PECC systems using optical microscopy.....19

Figure 10: Images of MPECC systems using optical microscopy.....19

Figure 11: Turbidity measurements of PECCs as a function of mole % polycation in the presence of 50ug/mL GOx.....20

Figure 12: Turbidity measurements of PECCs as a function of mole % polycation in the presence of 50ug/mL HRP.....21
Figure 13: Turbidity measurements of PECCs as a function of mole % polycation in the presence of 25ug/mL GOx and 25ug/mL HRP.....22
Figure 14: Encapsulation efficiency of 50ug/mL GOx by PECC systems. .....23
Figure 15: Encapsulation efficiency of 50ug/mL HRP by PECC systems. .....23
Figure 16: Encapsulation efficiency of 25ug/mL GOx and 25ug/mL HRP by PECC systems. ...23
Figure 17: Enzyme cascade activity and efficiency in a control system (pH 7 Water). No PECC or MPECC structures are present.....24
Figure 18: Michaelis-Menten graphs of the encapsulated enzyme cascade in PECC systems. ....25
Figure 19: Michaelis-Menten graphs of the encapsulated enzyme cascade in MPECC systems. The inner phase contains HRP while the outer phase contains GOx.....27
Figure 20: Michaelis-Menten graphs of the encapsulated enzyme cascade in MPECC systems. The inner phase contains GOx while the outer phase contains HRP.....27

# LIST OF TABLES

Table 1: Peptide patterns of polycations and polyanions used. Reproduced from Tabandeh et al. with permission from Molecules [19].....5

Table 2: Comparison of Km and Vmax values of the control and PECC systems.....25

Table 3: Comparison of Km and Vmax values of the control and MPECC systems. .....27

# LIST OF ABBREVIATIONS

1. PECCs: Polyelectrolyte complex coacervates
2. LLPS: Liquid-liquid phase separation
3. MPECCs: Multiphase polyelectrolyte complex coacervates
4. GOx: Glucose oxidase
5. HRP: Horseradish peroxidase

# LIST OF EQUATIONS

1. Turbidity at 500nm: $T = -\ln\left(\frac{I}{I_0}\right)$
2. Glucose oxidase standard curve equation: $y = -5 \times 10^{-6}x^2 + 0.0021x + 0.0045$
3. Horseradish peroxidase standard curve equation: $y = -6 \times 10^{-6}x^2 + 0.0024x + 0.0091$
4. Double-enzyme standard curve equation: $y = -5 \times 10^{-6}x^2 + 0.0023x + 0.0004$
5. Enzyme encapsulation efficiency equation: $\frac{Conc_{added} - Conc_{supernatant}}{Conc_{added}} * 100$

# CHAPTER 1: INTRODUCTION

Polyelectrolyte complex coacervates (PECCs) result from liquid-liquid phase separation (LLPS) in solutions containing oppositely charged polymers [1]. Electrostatic and hydrophobic interactions amongst the individual charged polymers and their environment drive PECCs to exist as liquid droplets when suspended in solution. When specific PECCs of differing interfacial tensions interact in solution, they form multiphase polyelectrolyte complex coacervates (MPECCs). MPECCs consist of two or more individual PECCs organized in a hierarchical fashion, with one existing within the other.

Enzyme encapsulation in PECCs and MPECCs can provide significant tools for the fields of drug manufacturing [6], green chemistry [7,8], material science [9], and synthetic cell biology [10]. In PECCs, enzymatic processes can be regulated to a single phase, diminishing interference from the environment. In MPECCs, distinct enzymatic processes can be localized to different phases, allowing for enzyme cascades to occur between phases. Enzyme encapsulation in MPECCs also serves to sharpen our understanding of synthetic cell biology, with a focus on membraneless organelles. Membraneless organelles have a structure very similar to that of either PECCs or MPECCs, depending on the structure of the membraneless organelle. Membraneless organelles dictate and regulate a multitude of related cellular reactions and enzymatic processes while also diminishing environmental interference. The self-assembly capabilities of both MPECCs and membraneless organelles via phase-separation allow for the encapsulation and localization of enzymes. Inter-phase reactions within MPECCs mimic the enzymatic structure of the nucleolus, a well-studied membraneless organelle.

The goal of this project is the successful encapsulation of two enzymes, horseradish peroxidase (HRP) and glucose oxidase (GOx), in both single phase (PECC) and multiphase (MPECC) biomimetic polyelectrolyte complexes. Once encapsulated, the enzymatic cascade between both enzymes will be evaluated for efficiency within either the PECC or MPECC. Successful encapsulation and efficiency of the enzymes illustrates the formation of a micron-sized biocatalytic reactor.

Practical applications for a micron-sized biocatalytic reactor are illustrated by the specificity of enzymes and their efficiency in product formation. Enzymes are a means of producing biofuels, medicines, and other chemical products in a more green, environmentally friendly way [8]. Compared to industrial chemical reactions that are not specific for a product, produce many side reactions, and incur substantial damage to the environment [11], enzymes are specific for their substrates, renewable, and make the same product with little to no side reactions occurring [12]. In an industrial setting, enzymes are susceptible to denaturation, which decreases their enzymatic efficiency. Micron-sized biocatalytic reactors serve to combat this phenomenon by encapsulating the enzyme(s) and protecting it/them from the outside environment. Thus mimicking the structured and efficient processes of the cell.

# CHAPTER 2: LITERATURE REVIEW

## 2.1: Polyelectrolyte Complex Coacervates

Polyelectrolyte complexation occurs when opposing charges on individual polyanionic and polycationic species interact with one another in an aqueous solution [13]. These polyanionic and polycationic species can be comprised of proteins, peptides, and/or polymers. This charge interaction leads to the phase-separation of either a solid-like or liquid-like material from the aqueous environment [14,15]. An image of both liquid-liquid phase separation and liquid-solid phase separation is illustrated below.

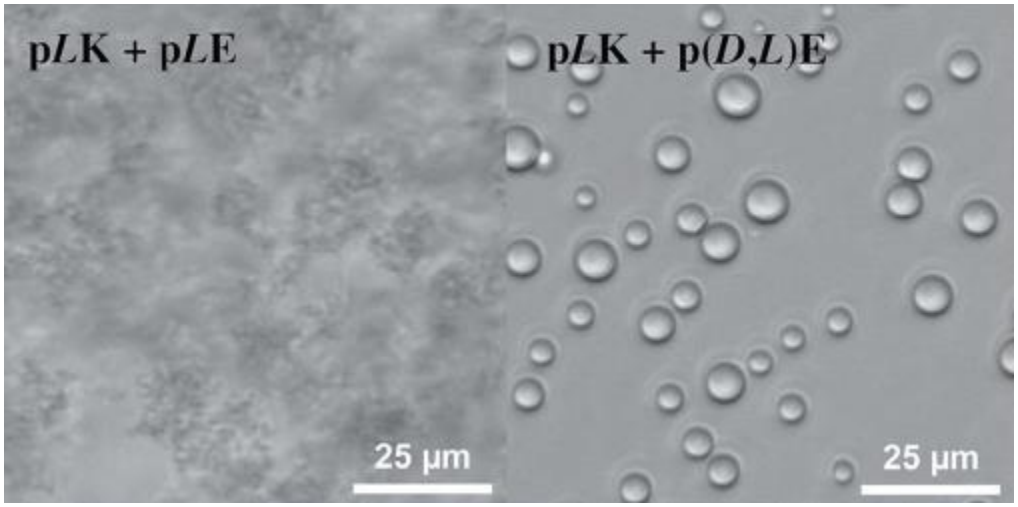


Figure 1: Illustration of both liquid-liquid phase separation (right) and liquid-solid phase separation (left). Reproduced from Marciel et al. with permission from Elsevier [16]

The level of complexation that occurs between the polycationic and polyanionic species is assessed using turbidity [17] . Once complexation has occurred, two phases are present within the solution: the complex phase (that is either solid-like or liquid-like) and the supernatant phase (which contains an extremely dilute concentration of complex or individual components) [18]. The liquid-like materials that phase-separate from solution are known as polyelectrolyte complex coacervates (PECCs) and initially appear as micro-sized spherical droplets. These droplets coalesce over time until they eventually form a separate phase via LLPS. PECCs tend to be

sensitive to changes in pH, salt concentration, temperature, ratio of polycation to polyanion, charge density, and total polymer concentration [19]. A remarkable property of PECCs is the extremely low interfacial tension between phases with the supernatant phase [20]. The interfacial tension between two liquids is calculated by assessing the free energy available per unit of surface area needed to generate the interface [21]. This ultra-low interfacial tension is responsible for many of the applications of PECCs in encapsulation technology (food industry [22], electronic ink [23], drug delivery [24]) and as underwater adhesives [25].

Using peptide based polyelectrolytes, the physical state (either liquid-like or solid-like) of the phase-separated structures can be predetermined by the chirality patterns of the polyanionic and polycationic species [26]. The chirality pattern of alternating D and L chiral amino acids in synthesized, charged polypeptide sequences allows for liquid-liquid phase separation to occur when these species are mixed in aqueous solution, generating PECCs [19,27]. Both racemic and perfectly alternating polypeptide sequences have been shown to form PECCs [27,28]. In contrast, when homochiral oppositely charged polypeptides are used, solid polyelectrolyte complexes form that contain hydrogen bonding between chains [28]. The alternating D-L patterns obstructs the formation of hydrogen bonds due to steric hinderance [28]. It is for that reason that the sequences used in this experiment consist of L and D chiral amino acids in an alternating fashion [19]. This alternating chirality pattern was accomplished using solid-phase peptide synthesis (SPPS) [19,29]. Charge density also plays an important role in the formation of PECCs. A higher charge density in both the polycation and polyanion species allows for increased electrostatic interactions between those charged species [30]. Hydrophobicity of amino acid side chains also plays a significant role in the formation of PECC systems. The bulky side chains associated with hydrophobic amino acids disrupts the formation of hydrogen bonds via steric hindrance [19]. This

hydrogen bond disruption prohibits the formation of beta-sheets, which are associated with solid precipitates [19].

For this project, the PECCs *p(kL)+p(eL), p(kKg)+p(eEg), p(kKl)+p(eEl),* and *p(kKa)+p(eEa),* which have been used in previous experiments of the Biomolecular Engineering Lab, were also used [19]. K refers to lysine, E to glutamic acid, G to glycine, A to alanine, and L to leucine. Lowercase letters are used to denote D-chiral amino acids, while uppercase letters are used to denote L-chiral amino acids. The p preceding each sequence stands for poly, illustrating that the sequences consist of multiple blocks. The first-generation sequences (*p(kL) and p(eL)*) consist of a heterochiral dimer block that is repeated 15 times [19]. The second-generation sequences (*p(kKg), p(eEg), p(kKa), p(eEa), p(kKl), and p(eEl)*) consist of a heterochiral hexamer block that is repeated 5 times [19]. The table below illustrates the chirality pattern of each peptide sequence, where X represents either glycine, alanine, or leucine.

| **Peptide Patterns** | **Polycations** | **Polyanions** |
|---|---|---|
| First Generation | $(kX)_{15}$ | $(eX)_{15}$ |
| Second Generation | $(kKxKkX)_5$ | $(eExEeX)_5$ |

Table 1: Peptide patterns of polycations and polyanions used. Reproduced from Tabandeh et al. with permission from Molecules [19].

Due to its preferred chirality pattern, high charge density, and incorporation of a high hydrophobic amino acid residue, preliminary data has shown that *p(kKl)+p(eEl)* produces more complex than the other PECC species at the same complex concentrations. Preliminary data of the Biomolecular Engineering Lab has also shown that *p(kL)+p(eL)* forms multiphase structures with *p(kKg)+p(eEg)* and *p(kKa)+p(eEa).* An image of a PECC that was formed using engineered peptides that follow the second-generation sequence pattern is shown below. NaCl was used as an aid to improve optical microscopy of the sample.

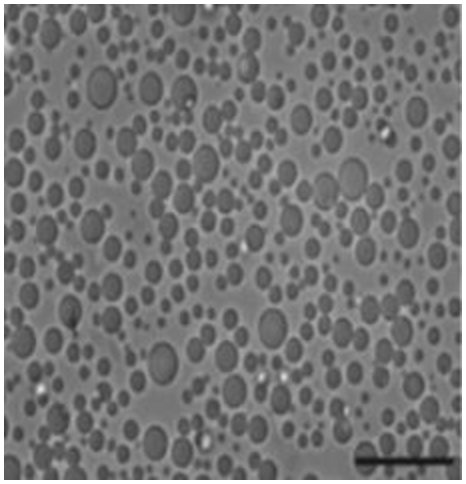

Figure 2: Image of p(kKa)+p(eEa) in 40mM NaCl. Reproduced from Tabandeh et al. with permission from Molecules [19].

PECCs have many similarities with membraneless organelles, which play important enzymatic and organizational roles within the cell [31,32]. Membraneless organelles are non-lipid enclosed, distinct droplets within a cell that also form via LLPS [33]. These organelles can be composed of RNA, proteins, peptides, or any non-lipid, charged cellular molecule [34]. Like synthetically engineered PECCs, membraneless organelles are known to coalesce to form larger structures [35]. Recent research has shown that the formation and dissolution of various membraneless organelles may also play a role in the progression of various diseases, such as cancer and neurodegenerative disease [36]. Recent studies have also shown that a phase transition of membraneless organelles from their liquid phase to an abnormal solid phase may be part of the progression of neurodegenerative diseases, such as ALS [37]. The biocompatibility of synthetically engineered PECCs is similar to that of cellular membraneless organelles [38]. This biocompatibility makes them excellent therapeutics delivery systems, synthetic cell research subjects, and/or blood-sugar regulators [39–41]. The encapsulation of glucose oxidase (GOx) in a biocompatible PECC suggests that these structures can be used to regulate blood sugar levels in diabetic patients [41,42]. The endocytosis of such PECCs by cells serves to illustrate their potential

as therapeutic drug vehicles as well [43]. The PECCs described thus far are indicative of single-phase polyelectrolyte complex coacervates. These same concepts can also be applied to multiphase polyelectrolyte complex coacervates (MPECCs).

## 2.2: Multiphase Polyelectrolyte Complex Coacervates

Multiphase complex coacervation can occur under multiple conditions. Some MPECCs can form when three polymers are mixed in solution, and subsequently form two phases due to varying affinities between polymers. Others can form if differing charged polymers from distinct coacervates prefer to interact with one another rather than interact with the charged polymers from their original coacervates. The previously stated methods for multiphase complexation are not the most common. The most common way polyelectrolyte multiphase complex coacervation occurs when one PECC is enveloped by, or envelopes, another [2,44]. Once this occurs, one PECC exists autonomously within the other. The formation of MPECCs due to envelopment works similarly to how individual PECCs are formed; however, there are slight distinctions. Individual PECCs must first be formed before multiphase complexation occurs. Once individual PECCs are formed, they are combined together to give rise to MPECCs [44]. The driving force behind polyelectrolyte multiphase complex coacervation lies in the differences in interfacial tension between the two PECCs [2]. The PECC with the higher interfacial tension is most likely to be engulfed by the other, leading to the formation of a MPECC [2].

Like PECCs, MPECCs have the ability to encapsulate different material; however, they also gain the ability to do so in distinct phases [45]. Such separation of phases allows for different processes to occur within a single MPECC, without the processes negatively interfering with one another. Images of various MPECCs are shown below.

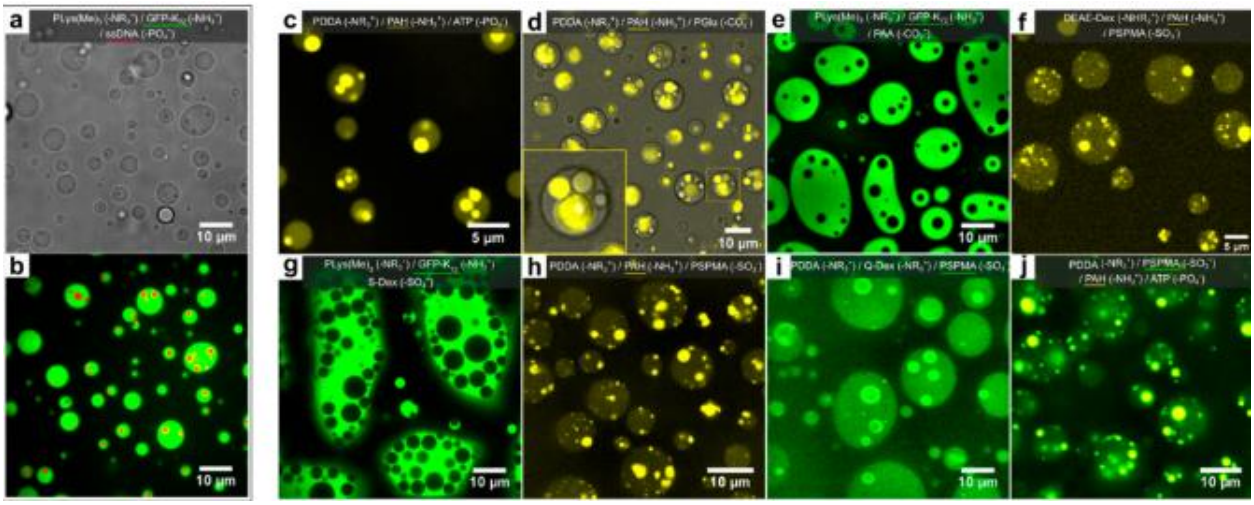

Figure 3: Images of multiphase complex coacervates formed via mixing various polymeric complex coacervates. Reproduced from Tiemei et al. from the Journal of the American Chemical Society [2].

In biological systems, multiphase complex coacervation occurs within certain membraneless organelles. One specific type of membraneless organelle in which multiphase complexation is well noted is the nucleolus [46]. The nucleolus has the ability to restrict distinct enzymatic processes, such as ribosomal assembly or rRNA transcription, to individual phases within its own multiphase structure [46]. The schematic of the nucleolus of the cell, shown as an MPECC, is illustrated below.

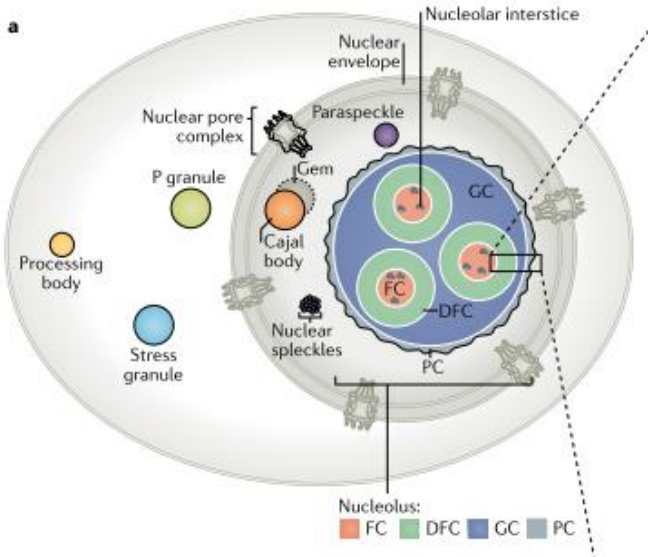


Figure 4: Schematic of the nucleolus illustrated as a multiphase complex coacervate. Reproduced from Lafontaine et al. with permission from Nature Reviews Molecular Cell Biology [46].

## 2.3: Encapsulation of Proteins/Enzymes

Single phase protein/enzyme encapsulation in PECCs is a rapidly developing area of research in the field of biomaterials. Enzymes are proteins that serve as biological catalysts, which facilitate in lowering the activation energy of a given reaction [5]. The encapsulation of enzymes allows for the localization and restriction of various enzymatic processes, while also diminishing the likelihood of environmental interference [47]. The efficiency of a PECC to encapsulate a protein/enzyme depends on the pH of the solution, the salt concentration of the solution, the length of the polyanion and polycation used, and the charge distribution/density of the protein/enzyme [4]. The pH and salt concentrations of a solution influence the ability of PECCs to encapsulate enzymes due to the interference on electrostatic interactions that results from changes in pH and/or salt concentration [4]. The length of the polyanion and polycation as well as the charge distribution/density of the enzyme to be encapsulated influence encapsulation via steric interactions [4]. Double phase protein/enzyme encapsulation in MPECCs is an area of research that has yet to be explored; however, this project explores just that.

Glucose oxidase (GOx), an enzyme with a net negative surface charge, catalyzes the oxidation of ß-D-glucose to D-glucono-δ-lactone and $H_2O_2$ [48,49]. This enzyme has been previously encapsulated by PECCs [41]. This encapsulation, along with the diffusion of ß-D-glucose into the PECC, allows for the oxidation of ß-D-glucose and production of $H_2O_2$ to occur within the PECC [41]. A schematic of that coacervate structure is seen below.

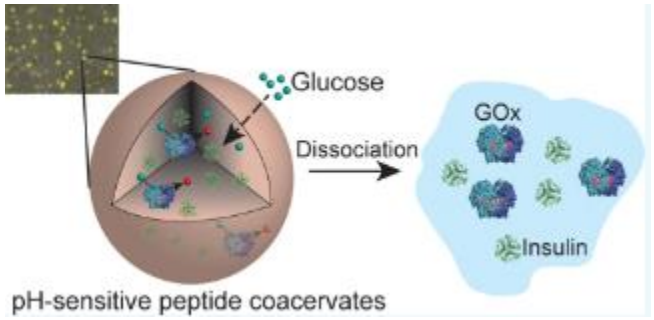


Figure 5: Encapsulation of glucose oxidase and insulin in a pH-sensitive complex coacervate. Reprinted from Lim et al. with permission from Bioconjugate Chemistry [41].

The encapsulation of horseradish peroxidase (HRP), an enzyme with a net positive charge [50] that catalyzes the conversion of chromogenic substrates in the presence of hydrogen peroxide [51], in PECCs has yet to be explored. Despite this, HRP has been encapsulated in peptide nanotubes [52], and has shown enzymatic activity while encapsulated. To illustrate enzymatic activity, a chromogenic reporter substrate must be used. The chosen chromogenic substrate for this experiment was 2,2′azino-bis (3-ethylbenzothiazoline-6-sulfonic acid (ABTS). In the presence of $H_2O_2$, HRP converts ABTS to its stable radical form, ABTS•+, which yields a blue/green color [51].

The phase distinction of enzymatic processes but exchange of products between phases can be assessed using a chromogenic substrate, such as ABTS. The HRP/ABTS [51] assay, along with the GOx-HRP enzyme cascade [53,54] allows for the quantitative analysis of the efficiency of the enzyme cascade in various phases. The GOx-HRP enzyme cascade is illustrated below.

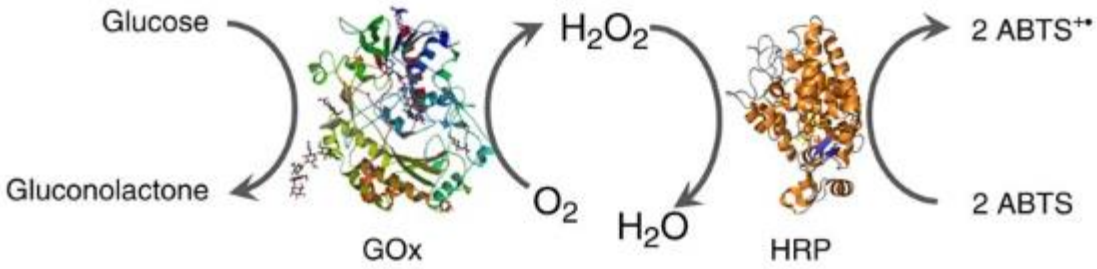


Figure 6: The GOx-HRP enzyme cascade and its quantification using ABTS. Reproduced from Zhang et al. with permission from Nature Communications [53].

The oxidation of ß-D-glucose to D-glucono-δ-lactone in the presence of $O_2$ [48,49] leads to the formation of $H_2O_2$, which is used by HRP to convert ABTS into its chromogenic state, ABTS•+ [53].

The encapsulation of GOx/HRP and the use of the ABTS assay to evaluate enzyme cascade efficiency illustrates the formation of enzymatically active PECC and MPECC models. Enzymatically active PECCs and MPECCs have a variety of uses ranging from cell-free chemical biosynthesis [8] to synthetic cell biology subjects [10]. This project explored the encapsulation of both GOx and HRP in PECC and MPECC models as well as the efficiency of the enzyme cascade once encapsulation occurred.

# CHAPTER 3: EXPERIMENTAL METHODOLOGY

## 3.1: Peptide-based PECC Stock Solutions

Previous work at Dr. Lorraine Leon's Biomolecular Engineering Lab has shown that the first-generation PECC *p(kL)+p(eL)* can form MPECCs with any one of the two second-generation PECCs: *p(kKg)+p(eEg)* and *p(kKa)+p(eEa)*. Turbidity experiments, enzyme uptake experiments, and enzyme activity/efficiency experiments were evaluated against both the individual PECCs as well as the MPECCs. Peptide stock solutions were made at both 10mM and 25mM with respect to monomer charge and stored at 4°C. Lyophilized peptide samples were kept at -20°C.

## 3.2: Enzyme Stock Solutions

Glucose oxidase (GOx) from *Aspergillus niger* and peroxidase from horseradish (HRP) were both purchased from Sigma Aldrich. Multiple aliquots of 250ug/mL concentration stock solution of both enzymes were made and stored at -20°C. Working stock solutions were taken out of -20°C and stored at 4°C for use. All experiments done using either enzyme were done in a dimly lit room, as both enzymes are photosensitive.

## 3.3: Turbidity Test

The first experiment of this project was designed to assess the turbidity of each individual PECC against three separate parameters: the presence of GOx, the presence of HRP, and the presence of a combination of the two enzymes. Samples were also tested at various percentages of polycation in the presence of enzyme to determine the ratio of polycation to polyanion in which complexation was the highest. Turbidity is defined by the equation below:

$$T = -\ln\left(\frac{I}{I_0}\right)$$

The turbidity is indicative of the degree of complexation that occurs in a sample.

Order of addition plays an important role in the outcome of this project. For samples containing only glucose oxidase, the following order of addition was used: 1) water, 2) glucose oxidase, 3) the polycationic peptide species, and 4) the polyanionic peptide species. For samples containing only horseradish peroxidase, the following order of addition was used: 1) water, 2) horseradish peroxidase, 3) the polyanionic peptide species, and 4) the polycationic peptide species. For samples containing both glucose oxidase and horseradish peroxidase, the following order of addition was used: 1) water, 2) glucose oxidase, 3) horseradish peroxidase, 4) the polycationic peptide species, and 5) the polyanionic peptide species.

The final 300uL solution of each PECC with enzyme met the following parameters: pH 7 water, 50ug/mL concentration of total enzyme, and 7mM PECC concentration with respect to monomer charge. Samples were made in 1.5mL microcentrifuge tubes (Eppendorf) and vortexed for 5 seconds. After samples were vortexed, 100uL of sample was immediately dispensed into 3 individual wells of a 96 well-plate (Costar, Corning Inc.) and read at 500nm.

A plate reader equipped with a UV-VIS spectrophotometer (Cytation5 imaging reader, Biotek Inc.) was used to measure turbidity of each sample. Turbidity was measured at 500nm, a wavelength that neither the complexes nor the enzymes absorbed at. This experiment was run in triplicates and error bars present represent the standard deviation of each sample.

## 3.4: Enzyme Encapsulation Efficiency

The second experiment of this project was designed to test the encapsulation efficiency of the individual PECCs for either GOx, HRP, or an equal combination of the two enzymes. The order of addition for each sample mirrored that seen in the turbidity experiments. The final 300uL solution of PECC with enzyme followed the given parameters: pH 7 water, 50ug/mL concentration of total enzyme, and 7mM PECC concentration with respect to monomer charge. Each solution was made in a 1.5mL microcentrifuge tube (Eppendorf), vortexed for 5 seconds, and left to complex for 20 minutes. After 20 minutes, samples were centrifuged (Thermo Scientific, Sorvall ST16R) at 13,000 rpm at 15°C for 30 minutes. As a blank measurement, samples of each PECC containing no enzyme were made and centrifuged.

160uL of the supernatant, post-centrifugation, of each sample was carefully removed, so as to not disturb the PECC pellet, and added to a separate 1.5mL microcentrifuge tube (Eppendorf). To each sample of supernatant, 160uL of Pierce Coomassie Plus (Bradford) Assay Reagent (ThermoFisher Scientific) was added, pipetting up and down to mix. 100uL of each sample was added to 3 wells of a 96 well-plate (Costar, Corning Inc.), to form triplicates, and the plate was left to incubate for 10 minutes. After incubation, samples were read at 595nm using a plate reader equipped with UV-VIS spectroscopy (Cytation5 imaging reader, Biotek Inc.). Blank measurements were subtracted from enzyme-containing measurements to ascertain the true absorbance of the enzyme in the supernatant.

To quantify the concentration of enzyme in the supernatant, three calibration curves were made: one for GOx, one for HRP, and one for an equal combination of both enzymes. A serial dilution of each curve, from 250ug/mL to 3.9ug/mL, was done in a 96 well-plate (Costar,

Corning Inc.) and an equal volume of Pierce Coomassie Plus (Bradford) Assay Reagent (ThermoFisher Scientific) was added and mixed into each well. After a 10-minute incubation period, absorbance of the plate was read at 595nm using the same methods and instruments as before.

The absorbance data of each serial dilution was used to create a standard curve. Inputting the absorbance data of the samples into their given standard curve equation calculated the concentration of enzyme that was left in the supernatant. Encapsulation efficiency of each PECC for either GOx, HRP, or an equal combination of the two enzymes was then calculated using the data collected. The equation for encapsulation efficiency is as follows:

$$EE\% = \frac{Conc_{added} - Conc_{supernatant}}{Conc_{added}} * 100$$

Samples and calibration curves were run in triplicates and error bars shown indicate the standard deviation of each data set.

### 3.5 Enzyme Cascade Activity and Efficiency

The final experiment for this project was designed to evaluate the activity and efficiency of the encapsulated enzyme cascade. Enzymatic activity and efficiency were tested both in PECC and MPECC models. PECC and MPECC systems were formed in a 96 well-plate (Costar, Corning Inc.) and pipetted up and down to facilitate mixing. This portion of the project relied both on the GOx-HRP enzyme cascade and the ABTS assay. ABTS was purchased from Sigma Aldrich in tablet form. The ABTS assay is generally spectroscopic in nature; however, since the PECC and MPECC systems scatter light, this method cannot be used. To evaluate the enzyme

cascade's efficiency and activity, optical microscopy was used to track the chromogenic change in intensity over time.

PECC samples were made at a final volume of 100uL. The order of addition used for PECC samples, which contained both enzymes, was as follows: 1) water at pH 7, 2) glucose oxidase at 25ug/mL, 3) horseradish peroxidase at 25ug/mL, 4) ABTS at 300uM, 5) the polycationic peptide species, 6) the polyanionic peptide species, and 7) glucose ranging from 0 to 1000uM. Complexes were made at a final concentration of 7mM with respect to monomer charge. The order of addition for MPECC samples depended on which enzyme was to be allocated to a particular phase. The schematic for MPECC sample formation can be found below.


Figure 7: Enzyme cascade activity and efficiency schematic for MPECC samples.

Individual complexes for MPECC formation were made at 100uL and a concentration of 7mM with respect to monomer charge. Half of each individual complex was added to a single well to form MPECC structures. For MPECC samples, phases were made independently of one another, then combined to form multiphase structures. For MPECC phases containing glucose oxidase, the following order of addition was used: 1) water at pH 7, 2) glucose oxidase at 50ug/mL, 3) ABTS at 300uM, 4) the polycationic peptide species, 5) the polyanionic peptide

species, and 6) glucose ranging from 0 to 1000uM. For MPECC phases containing horseradish peroxidase, the following order of addition was used: 1) water at pH 7, 2) horseradish peroxidase at 50ug/mL, 3) ABTS at 300uM, 4) the polyanionic peptide species, 5) the polycationic peptide species, and 6) glucose ranging from 0 to 1000uM.

ImageJ was used to quantify the color intensity of coacervate samples at different time points for each of the PECC and MPECC systems at various concentrations of glucose. Once quantified, the initial velocity of each reaction was calculated and plotted against the glucose concentration for that sample. From this, a Michaelis-Menten graph was formed. An example of a Michaelis-Menten graph is illustrated below.

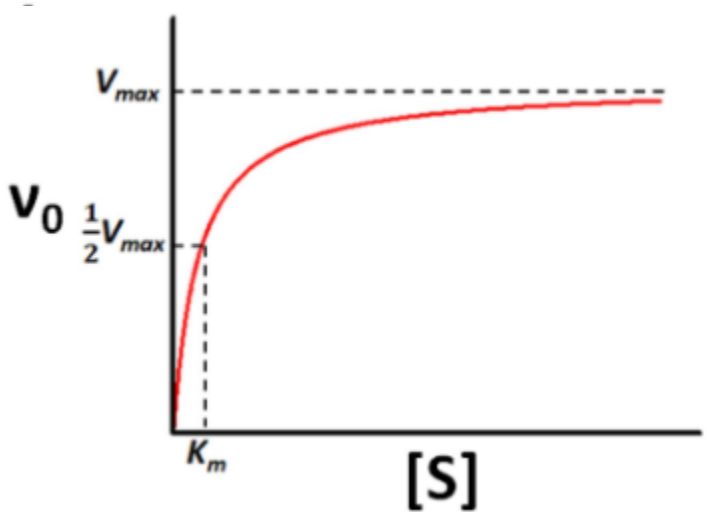


Figure 8: Michaelis-Menten kinetics graphical representation. The initial velocity ($v_0$) is plotted against substrate concentration ([S]). $V_{max}$ and $K_m$ can be calculated from the graph. Reproduced from Wang et al. with permission from Frontiers [57].

Michaelis-Menten enzyme kinetics describes enzymatic processes as steady-state reactions. Steady-state reactivity refers to the process in which the enzyme-substrate intermediates are formed and consumed at identical rates, assuming that the substrates, enzymes, and enzyme-substrate intermediates are at equilibrium [55]. Enzyme reactivity within PECC and MPECC systems followed Michaelis-Menten kinetics, illustrating that encapsulated reactions

occur in a steady-state fashion. A Michaelis-Menten graph plots the initial rate of an enzymatic reaction against the concentration of substrate used for that reaction. This graph, which produces a sigmoidal curve, will begin to plateau as the enzyme cascade reaches saturation. From this graph, two constants can be calculated: $K_m$ and $V_{max}$. The $K_m$ value illustrates the substrate concentration at which the reaction rate is 50% of $V_{max}$. Lower $K_m$ values illustrate higher enzyme-substrate affinity, while higher $K_m$ values illustrate lower enzyme-substrate affinity. The $V_{max}$ illustrates the rate of reaction when the enzyme(s) is/are completely saturated with substrate. Lower $V_{max}$ values illustrate faster enzyme-substrate saturation, while higher $V_{max}$ values illustrate slower enzyme-substrate saturation [56].

# CHAPTER 4: RESULTS AND DISCUSSION

## 4.1: Optical Microscopy of PECC and MPECC Systems

*p(kKg)+p(eEg)*

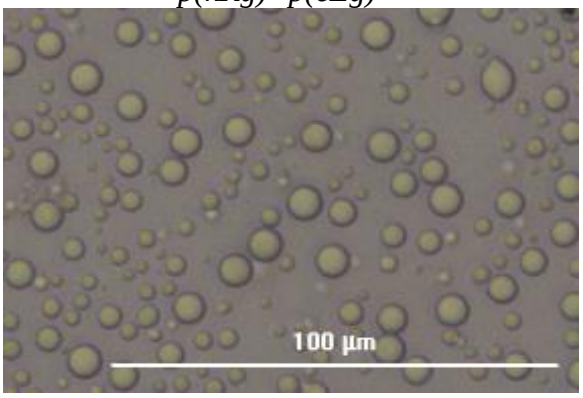


*p(kKa)+p(eEa)*

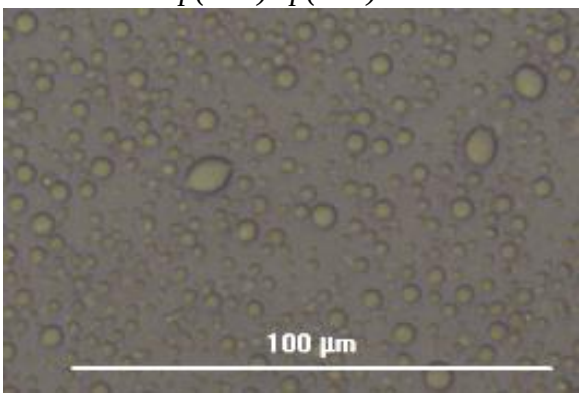


*p(kKl)+p(eEl)*

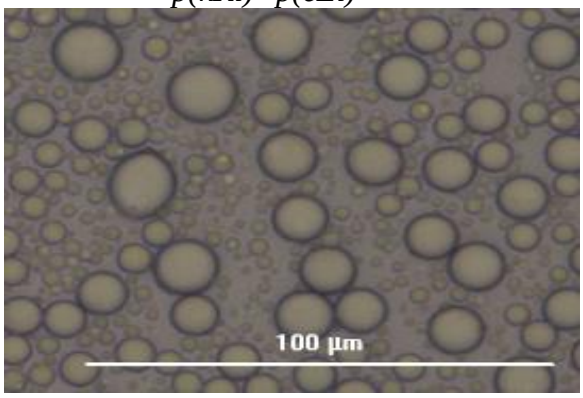


*p(kL)+p(eL)*

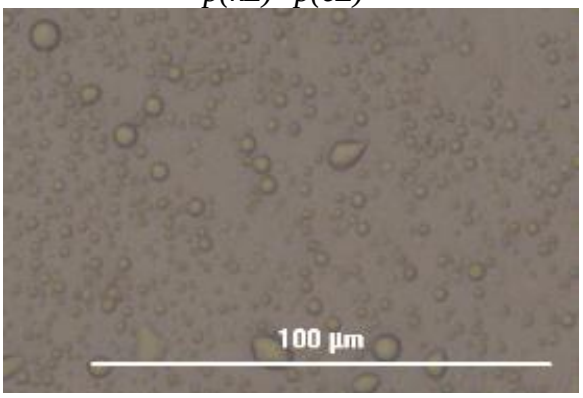


Figure 9: Images of PECC systems using optical microscopy.

*p(kKg)+p(eEg) + p(kL)+p(eL)*

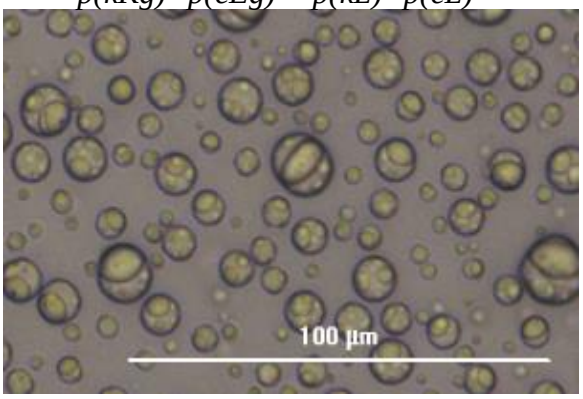


*p(kKa)+p(eEa) + p(kL)+p(eL)*

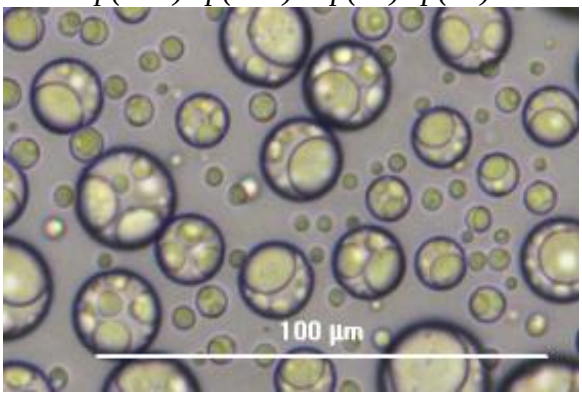


Figure 10: Images of MPECC systems using optical microscopy.

Both figure 9 and figure 10 illustrate PECC and MPECC systems existing as liquid coacervate droplets suspended in supernatant. All PECC and MPECC systems pictured above were made at 7mM with respect to monomer charge. Images were taken 20 minutes after formation. Of the PECC systems presented, seen in figure 9, *p(kKl)+p(eEl)* forms the most complex compared to all other PECC systems. The MPECC systems presented, seen in figure 10, are composed of two individual PECCs. For both *p(kKg)+p(eEg)* + *p(kL)+p(eL)* and *p(kKa)+p(eEa)* + *p(kL)+p(eL)* MPECC systems, *p(kL)+p(eL)* exists as the inner phase.

## 4.2: Degree of Turbidity as a Function of Percent mole Polycation

Turbidity experiments without enzyme illustrate that the highest turbidity occurs at 50% polycation to polyanion [19]. This suggests that a 1:1 stoichiometric charge ratio is required to obtain maximum complexation without the presence of enzyme.

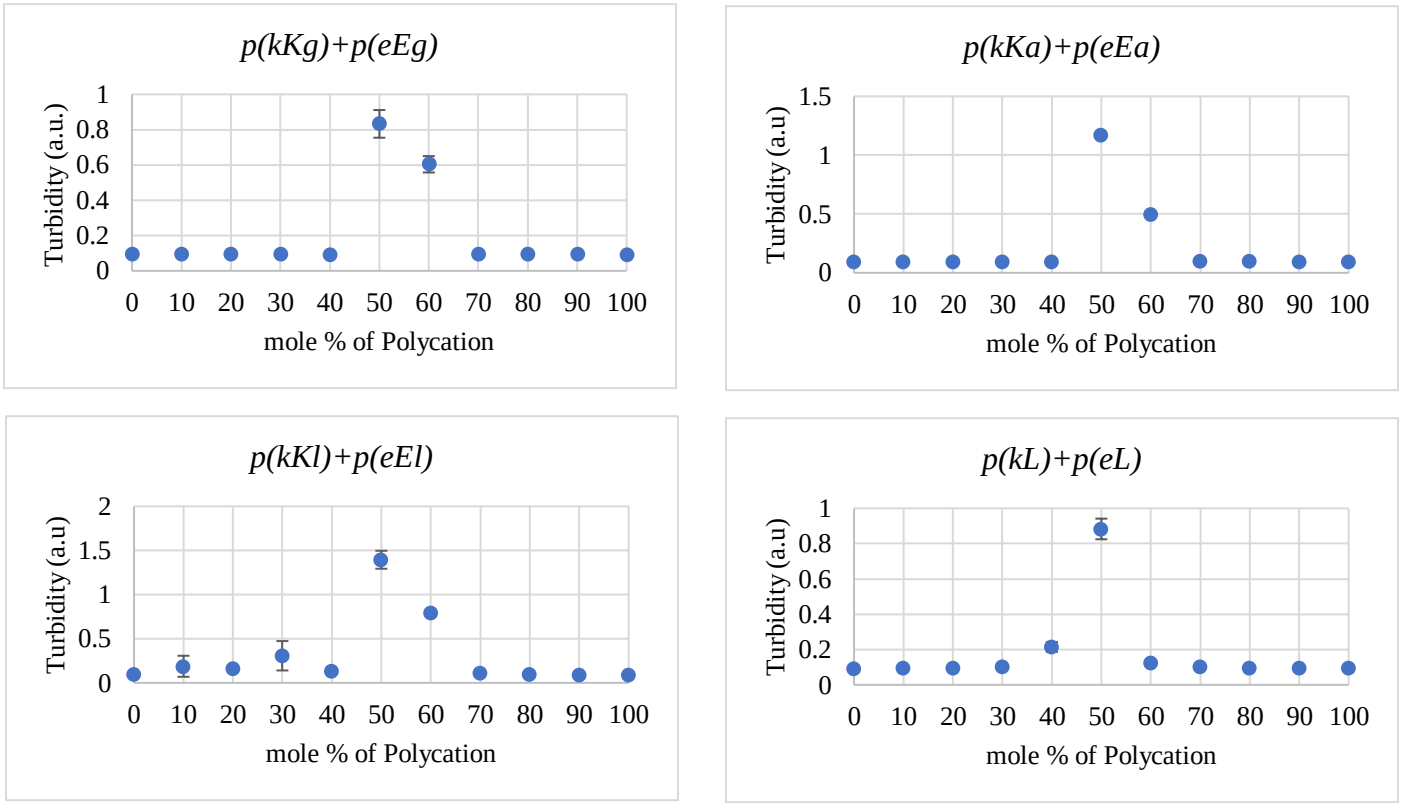


Figure 11: Turbidity measurements of PECCs as a function of mole % polycation in the presence of 50ug/mL GOx

For GOx containing samples, figure 11, highest turbidity occurred at 50% polycation to polyanion. This suggests that in the presence of GOx, an enzyme with a net negative surface charge, a 1:1 stoichiometric charge ratio leads to maximum complex formation. The net negative surface charge of GOx did not shift the degree of turbidity compared to a non-enzyme containing sample. This suggests that the concentration of GOx, 50ug/mL, is too low to affect the maximum turbidity of the PECC systems.

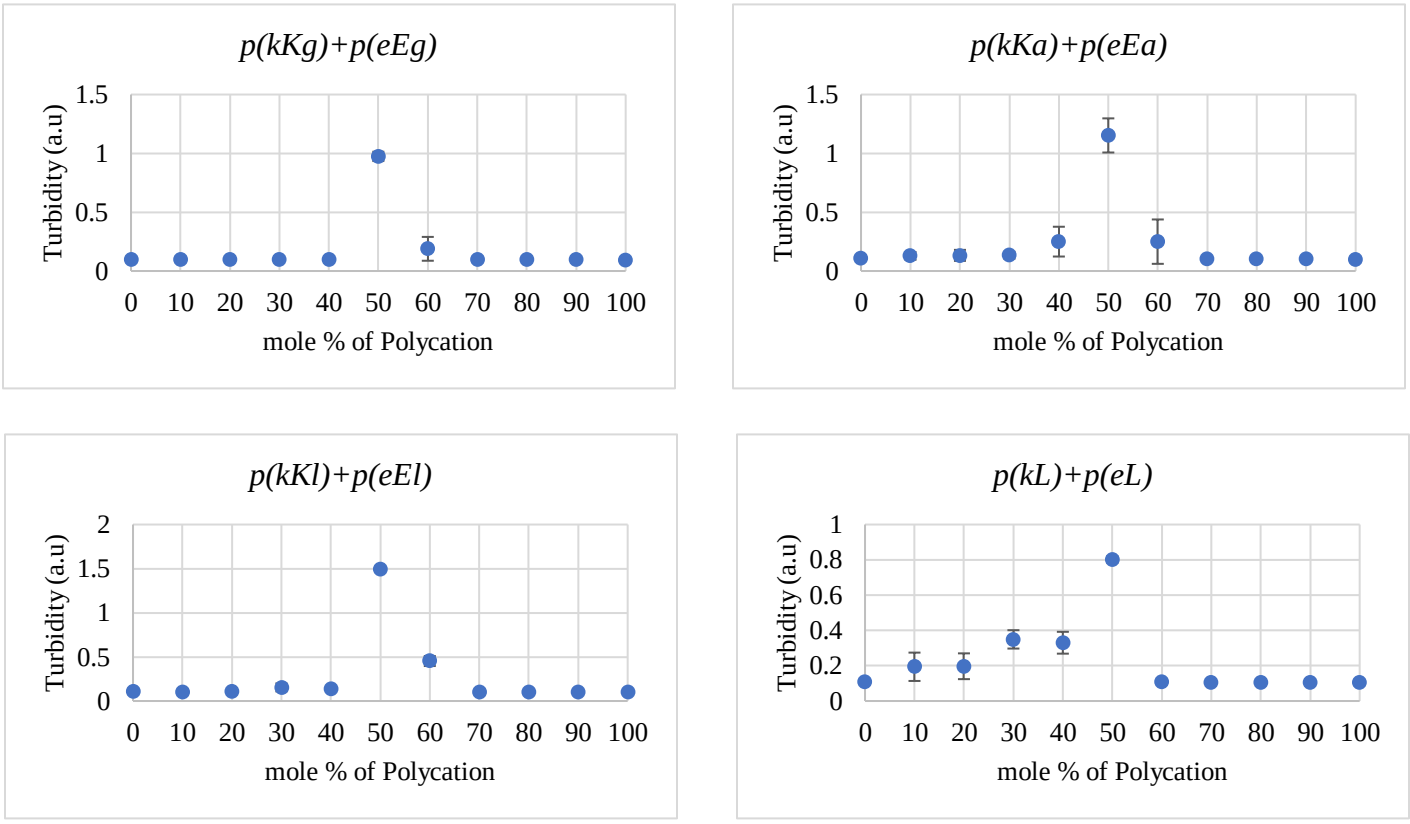


Figure 12: Turbidity measurements of PECCs as a function of mole % polycation in the presence of 50ug/mL HRP.

For HRP containing samples, figure 12, highest turbidity also occurred at 50% polycation to polyanion, suggesting a 1:1 stoichiometric charge ratio in the presence of an enzyme with a net positive surface charge. The net positive surface charge of HRP did not shift the degree of

turbidity compared to a non-enzyme containing sample. This suggests that, like for GOx, the concentration of HRP is too low to affect the maximum turbidity of the PECC systems.

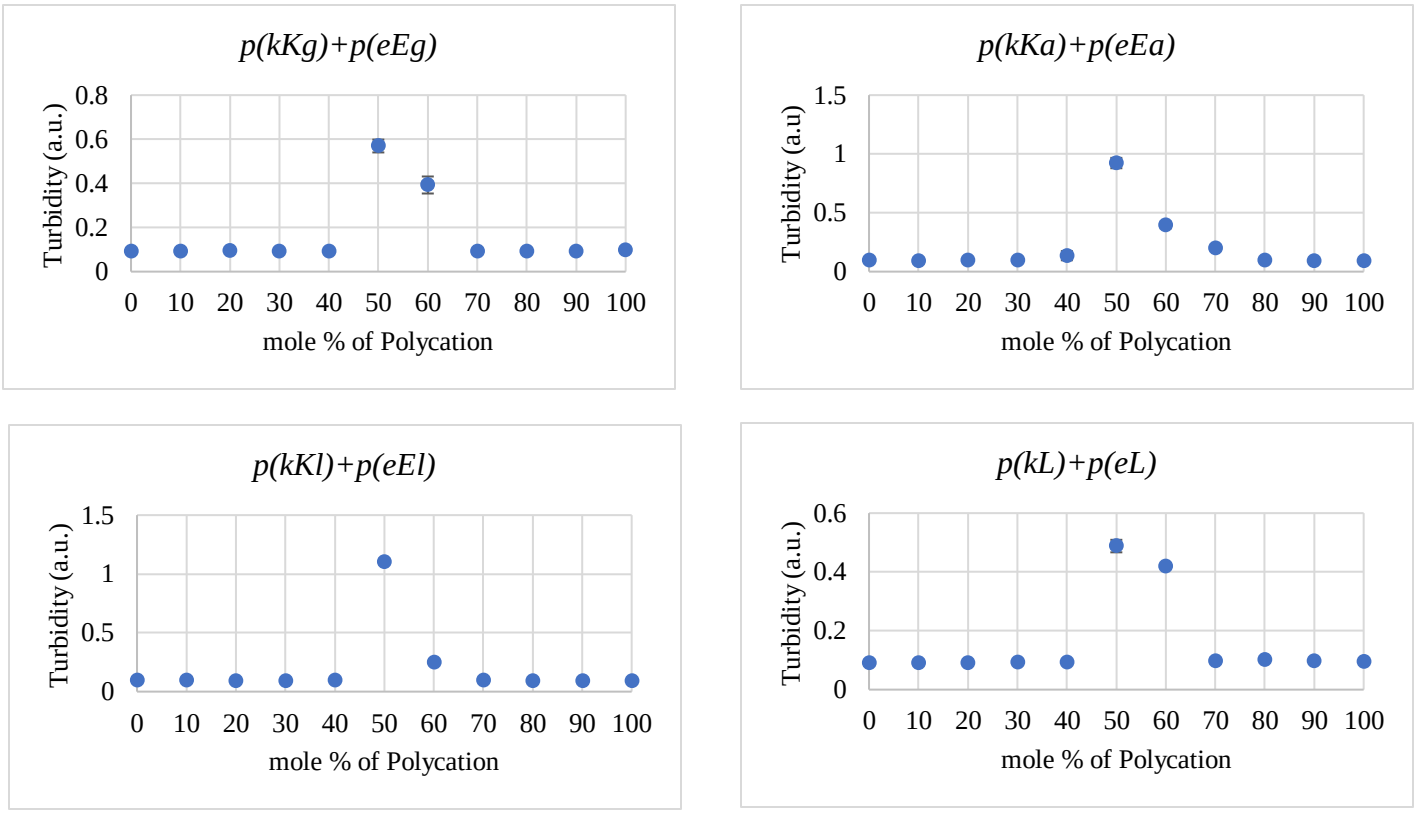


Figure 13: Turbidity measurements of PECCs as a function of mole % polycation in the presence of 25ug/mL GOx and 25ug/mL HRP.

For samples containing an equal concentration of GOx and HRP, figure 13, highest turbidity is also seen at 50% polycation to polyanion, suggesting that a 1:1 stoichiometric charge ratio is needed for maximum complexation. The presence of both a negative surface charge and positive surface charge enzyme does not affect the maximum turbidity of PECC systems, compared to a non-enzyme containing PECC system. This suggests that the concentration of both enzymes was too low to affect maximum turbidity.

## 4.3: Encapsulation Efficiency of Enzymes by PECCs

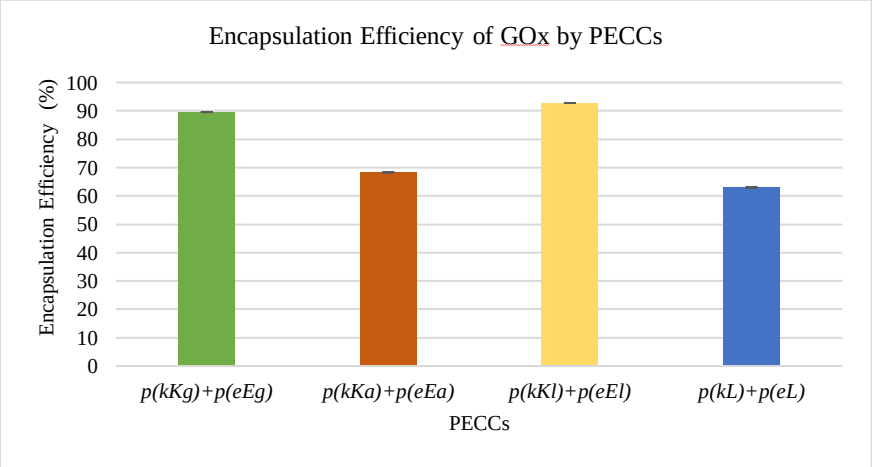


Figure 14: Encapsulation efficiency of 50ug/mL GOx by PECC systems.

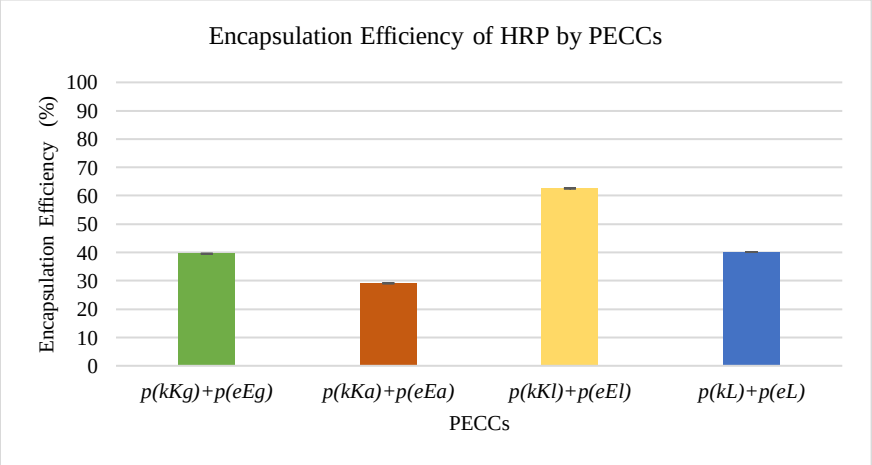


Figure 15: Encapsulation efficiency of 50ug/mL HRP by PECC systems.

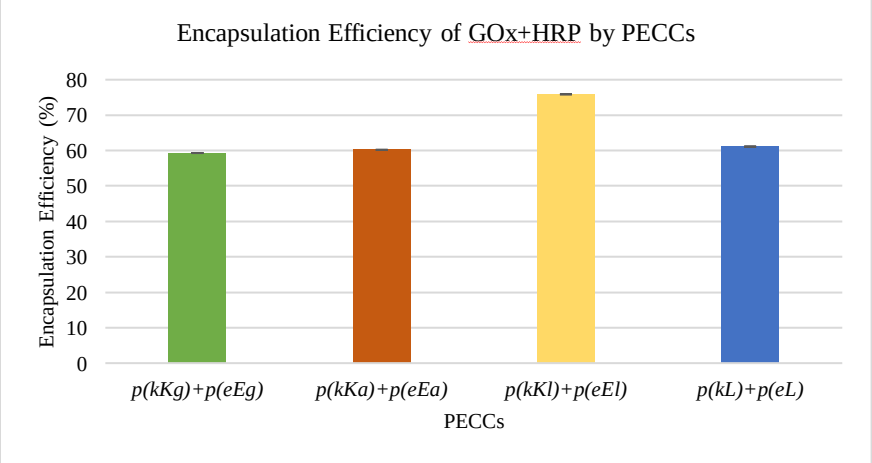


Figure 16: Encapsulation efficiency of 25ug/mL GOx and 25ug/mL HRP by PECC systems.

Encapsulation efficiency of GOx, HRP, and an equal combination of the two enzymes was evaluated against all four PECC systems, figures 14-16. Each PECC system illustrated a higher encapsulation efficiency percentage for GOx compared to HRP. The reason for this is currently unknown; however, it is hypothesized that it may be due to the surface charge difference between the two enzymes.

Of the four PECC systems, *p(kKl)+p(eEl)* had the highest encapsulation efficiency percentage of GOx, HRP, and an equal combination of the two enzymes. Preliminary data illustrates that do to its advantageous chirality pattern, charge density, and incorporation of a high hydrophobic amino acid residue, *p(kKl)+p(eEl)* forms the most complex, compared to other PECC systems, at the same complex concentrations. This suggests that because it forms the most complex, *p(kKl)+p(eEl)* has the capacity to encapsulate more enzyme.

## 4.4: Enzyme Cascade Activity and Efficiency in PECC Systems

PECC and MPECC enzyme kinetics relied on the enzymatic reaction occurring within the systems and the diffusion of glucose into that PECC/MPECC. The kinetics calculated represent the activity of the reaction within the system as well as the diffusion of glucose into that system.

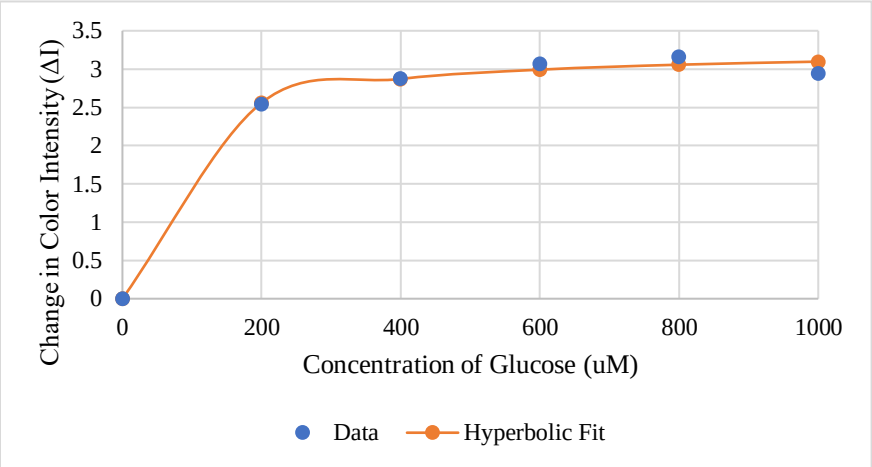


Figure 17: Enzyme cascade activity and efficiency in a control system (pH 7 Water). No PECC or MPECC structures are present.

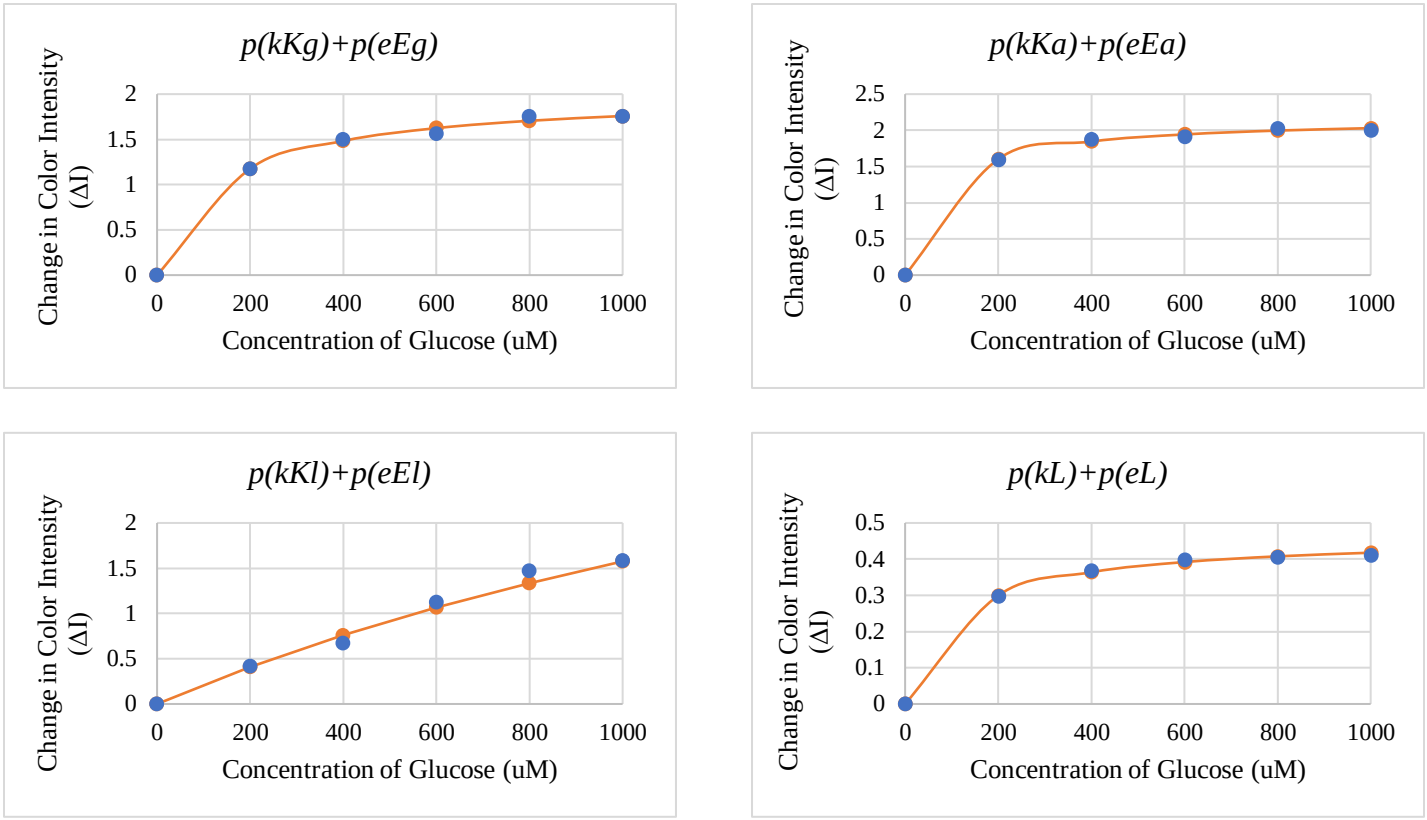


Figure 18: Michaelis-Menten graphs of the encapsulated enzyme cascade in PECC systems.

| **PECC** | **$K_m$** | **$V_{max}$** |
|---|---|---|
| Control | 55.49 uM | 3.27 ΔI $s^{-1}$ |
| *p(kKg)+p(eEg)* | 141.41 uM | 2.01 ΔI $s^{-1}$ |
| *p(kKa)+p(eEa)* | 71.67 uM | 2.18 ΔI $s^{-1}$ |
| *p(kKl)+p(eEl)* | 2485.01 uM | 5.49 ΔI $s^{-1}$ |
| *p(kL)+p(eL)* | 109.79 uM | 0.463 ΔI $s^{-1}$ |

Table 2: Comparison of Km and Vmax values of the control and PECC systems.

For PECC systems, Michaelis-Menten graphs, figure 18, were formed to illustrate that the enzyme cascade still followed general enzyme kinetics, despite being encapsulated. For this experiment, $K_m$ served as an understanding for enzyme-substrate affinity within a PECC system.

$V_{max}$ served as an understanding for the speed at which the enzyme cascade occurred within the PECC system. Compared to the control ($K_m$ = 55.49uM), all PECC systems had higher $K_m$ values, illustrating that enzyme-substrate affinity is lower within PECC systems compared to just in pH 7 water. We hypothesize that this occurs because in PECC systems, both enzymes and substrates are initially present in separate phases, whereas in water, enzymes and substrates are initially present in the same phase. Among the PECC systems, $K_m$ was significantly lowest in *p(kKa)+p(eEa)* ($K_m$ = 71.67uM). This illustrates that the enzyme cascade between GOx and HRP has the highest affinity for their associated substrates within *p(kKa)+p(eEa).* This suggests that either enzyme and/or substrate can diffuse and travel more easily within that PECC compared to the others. We hypothesize that the enzymes, GOx and HRP, and the substrates, glucose and ABTS, can travel more easily within *p(kKa)+p(eEa)* due to the PECC's slight hydrophobic nature. Enzymatic reactions that take place in slightly hydrophobic environments tend to have higher enzyme-substrate affinities than in hydrophilic environments [58]. The $V_{max}$ varied among the control and PECC groups. The enzyme cascade reached saturation faster when in *p(kL)+p(eL)* ($V_{max}$ = 0.463 $\Delta I\ s^{-1}$) compared to all other PECCs and the control ($V_{max}$ = 3.27 $\Delta I\ s^{-1}$). Optical microscopy demonstrates that *p(kL)+p(eL)* forms the smallest PECC in terms of its diameter. We hypothesize that, due to the complex's smaller size, encapsulated enzymes become more saturated with substrate due to the decreased distance between enzyme and substrates. The inverse is true and is illustrated in *p(kKl)+p(eEl)* ($V_{max}$ = 5.48 $\Delta I\ s^{-1}$). Optical microscopy demonstrates that *p(kKl)+p(eEl)* forms the largest PECC in terms of its diameter. Due to the complex's larger size, encapsulated enzymes become less saturated with substrate due to the increased distance between enzyme and substrate.

## 4.5: Enzyme Cascade Activity and Efficiency in MPECC Systems

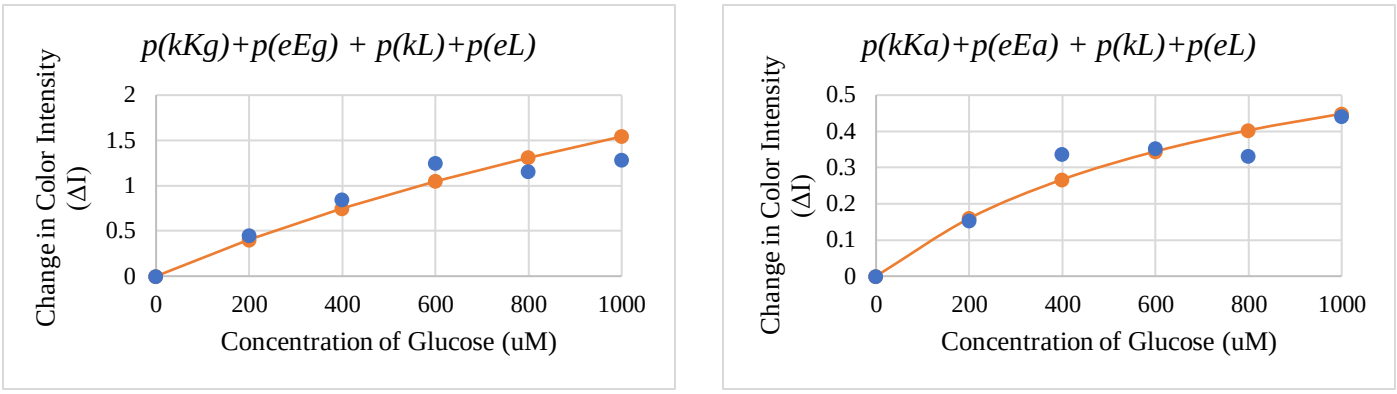


Figure 19: Michaelis-Menten graphs of the encapsulated enzyme cascade in MPECC systems. The inner phase contains HRP while the outer phase contains GOx.

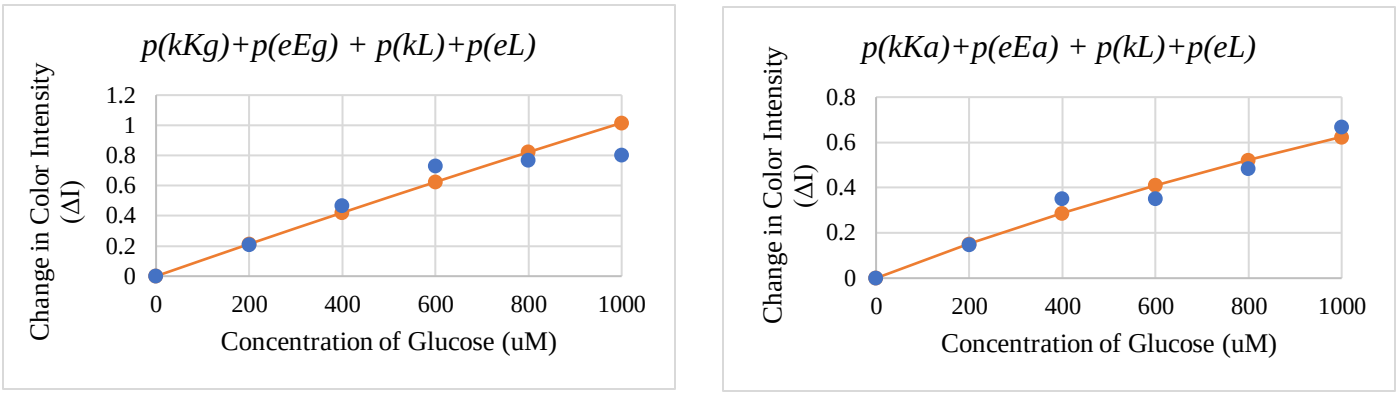


Figure 20: Michaelis-Menten graphs of the encapsulated enzyme cascade in MPECC systems. The inner phase contains GOx while the outer phase contains HRP.

| Scenario | Complex | Km | Vmax |
|---|---|---|---|
| N/A | Control | 55.49 uM | 3.27 $\Delta I\ s^{-1}$ |
| Inner Phase Contains HRP | *p(kKg)+p(eEg) + p(kL)+p(eL)* | 2437.169 uM | 5.30 $\Delta I\ s^{-1}$ |
| | *p(kKa)+p(eEa) + p(kL)+p(eL)* | 829.19 uM | 0.820 $\Delta I\ s^{-1}$ |
| Inner Phase Contains GOx | *p(kKg)+p(eEg) + p(kL)+p(eL)* | 16636.38 uM | 17.92 $\Delta I\ s^{-1}$ |
| | *p(kKa)+p(eEa) + p(kL)+p(eL)* | 3523.016 uM | 2.82 $\Delta I\ s^{-1}$ |

Table 3: Comparison of Km and Vmax values of the control and MPECC systems.

Michaelis-Menten graphs were formed for MPECC systems based on the location of a particular enzyme in a particular phase of the multiphase structure. Michaelis-Menten graphs for MPECC systems containing HRP in the inner phase, figure 19, were formed to demonstrate that the enzyme cascade still follows general enzyme kinetics while encapsulated. The same general enzyme kinetics is seen in systems that contained GOx in the inner phase, figure 20. $K_m$ and $V_{max}$ were calculated to assess the enzyme cascade efficiency within the multiphase structure. Samples with GOx in the inner phase have a significantly higher $K_m$ and $V_{max}$ compared to samples with HRP in the inner phase. This is because glucose must diffuse through two phases before interacting with GOx in the former compared to one phase in the latter. Allocating GOx to the inner phase made the enzymatic cascade less efficient. PECC enzyme cascade efficiency experiments demonstrated that *p(kKa)+p(eEa)* allowed for an easier diffusion and movement of enzymes and substrates within that PECC system. The same is true for MPECC systems, in which all MPECCs containing *p(kKa)+p(eEa)* have a lower $K_m$ than their *p(kKg)+p(eEg)* comparisons. PECC enzyme cascade efficiency experiments also showed that *p(kL)+p(eL)* has a lower $V_{max}$ due to its decreased diameter. This holds true in MPECC systems as well, as enzymes are allowed to reach saturation faster.

MPECC systems have a unique advantage over PECC systems in that the enzyme cascade is organized within two distinct phases. The allocation of GOx and HRP into distinct phases of an MPECC allows the system to have the combinatorial benefits of multiple PECCs, which individual PECC systems lack. This idea is demonstrated in the *p(kKa)+p(eEa) + p(kL)+p(eL)* MPECC system. Enzyme activity and efficiency data in PECC systems illustrate that *p(kKa)+p(eEa)* allows for the highest enzyme-substrate affinity while *p(kL)+p(eL)* allows for the fastest enzyme-substrate saturation. The MPECC produced from these two PECCs,

*p(kKa)+p(eEa) + p(kL)+p(eL),* obtains both the high enzyme-substrate affinity as well as the faster enzyme-substrate saturation in both GOx inner phase and HRP inner phase experiments when compared to the *p(kKg)+p(eEg) + p(kL)+p(eL)* systems. MPECC systems prove to be advantageous as they possess the cumulative benefits of their individual PECC parts.

# CHAPTER 5: CONCLUSION

Overall, this research serves as a possible micron-sized biocatalytic reactor for the industrial use of enzymes. Enzymes are often used to produce biofuels, medicines, and a variety of other necessary chemicals. Compared to traditional industrial chemical reactions, enzymes serve as a green, environmentally conscious means of production. In an industry setting however, enzymes are often subject to denaturation or sub-optimal conditions, hindering their output and performance. Micron-sized biocatalytic reactors serve to combat this phenomenon by encapsulating the enzyme(s), protecting it/them from the outside environment. This project suggests two structures, single phase and multiphase, that can be used to encapsulate multiple enzymes and initiate and sustain an enzyme cascade.

Maximum turbidity of PECC systems did not shift, despite the addition of charged enzymes. It was thought that the addition of charged enzymes may interfere with the electrostatic interactions between polycationic and polyanionic species; however, the concentration of enzyme was too low to interfere with complexation. Maximum turbidity was still seen at 50% polycation to polyanion, suggesting that a 1:1 stoichiometric charge ratio is ideal for PECC formation.

Encapsulation efficiency of GOx by PECCs was significantly higher than that of HRP. The reason for which is unknown, but it is hypothesized that it is due to the charge difference between the two enzymes. Due to its high level of complexation, *p(kKl)+p(eEl)* proved to be the best PECC at encapsulation of both enzymes.

The GOx-HRP enzyme cascade had the highest enzyme-substrate affinity in the *p(kKa)+p(eEa)* PECC. This high affinity suggests that both the enzymes and/or substrates can

diffuse and move more easily within this PECC system compared to the other systems. The enzyme cascade had the fastest enzyme-substrate saturation in the *p(kL)+p(eL)* PECC. This fast enzyme-substrate saturation suggests that the smaller size of *p(kL)+p(eL)* allows for less space between the enzymes and their substrates, leading to earlier saturation. The GOx-HRP enzyme cascade in MPECC systems illustrates the cumulative qualities of MPECCs. MPECC systems obtain all distinct attributes of the individual PECC systems that comprise them. The MPECC system *p(kKa)+p(eEa) + p(kL)+p(eL)* is a prime example of that idea. Compared to the MPECC *p(kKg)+p(eEg) + p(kL)+p(eL), p(kKa)+p(eEa) + p(kL)+p(eL)* allows for both a higher enzyme-substrate affinity as well as a faster enzyme-substrate saturation.

This research illustrates the advantageous uses of PECC and MPECC systems in encapsulating enzymatic cascades. Compared to water, PECC and MPECC systems allow for the encapsulation and insulation of enzymatic activity, ensuring that external environmental factors are minimized. PECC systems serve as promising vehicles for enzyme-cascades, however they come with limitations. One such limitation is that they lack organization. PECC systems are not able to allocate specific enzymes to distinct phases. MPECC systems, however, can do just that. An added benefit to MPECC systems is that they obtain all the desired qualities of the PECC systems that comprise them. Both PECC and MPECC systems illustrate promising outcomes for the encapsulation of enzymatic reactions.

# CHAPTER 6: FURTHER STUDIES

Following the research done in this project, there are several investigations that can be done to further the understanding of this topic. One such investigation is assessing why glucose oxidase can be encapsulated at a higher rate than horseradish peroxidase by all PECC systems. It was hypothesized that due to its net negative surface charge, glucose oxidase is more easily encapsulated; however, that is merely a hypothesis. Other aspects that could affect this encapsulation difference are the respective size of the enzymes and the hydrophobicity or hydrophilicity of the external amino acid residues.

Another investigation that can be done is to assess the degree of turbidity of all PECC systems in the presence of glucose and ABTS. This will illustrate if those two molecules shift/affect the maximum turbidity of each PECC system.

Future studies could also assess why the enzymes used and their corresponding substrates have a higher affinity for one another in the *p(kKa)+p(eEa)* system compared to the other PECC systems. This can also be assessed in MPECC systems that contain *p(kKa)+p(eEa),* as the high affinity is seen in those cases as well.

REFERENCES


(1) Chen, S.; Wang, Z.-G. Driving Force and Pathway in Polyelectrolyte Complex Coacervation. *Proc. Natl. Acad. Sci.* **2022**, *119* (36), e2209975119. https://doi.org/10.1073/pnas.2209975119.

(2) *Multiphase Complex Coacervate Droplets | Journal of the American Chemical Society*. https://pubs.acs.org/doi/10.1021/jacs.9b11468 (accessed 2023-04-09).

(3) *Protein Encapsulation via Polypeptide Complex Coacervation | ACS Macro Letters*. https://pubs.acs.org/doi/10.1021/mz500529v (accessed 2023-04-09).

(4) *Design rules for encapsulating proteins into complex coacervates - Soft Matter (RSC Publishing)*. https://pubs.rsc.org/en/content/articlelanding/2019/sm/c9sm00372j (accessed 2023-04-09).

(5) Robinson, P. K. Enzymes: Principles and Biotechnological Applications. *Essays Biochem.* **2015**, *59*, 1–41. https://doi.org/10.1042/bse0590001.

(6) Moura, M.; Finkle, J.; Stainbrook, S.; Greene, J.; Broadbelt, L. J.; Tyo, K. E. J. Evaluating Enzymatic Synthesis of Small Molecule Drugs. *Metab. Eng.* **2016**, *33*, 138–147. https://doi.org/10.1016/j.ymben.2015.11.006.

(7) Chapman, J.; Ismail, A. E.; Dinu, C. Z. Industrial Applications of Enzymes: Recent Advances, Techniques, and Outlooks. *Catalysts* **2018**, *8* (6), 238. https://doi.org/10.3390/catal8060238.

(8) Wilding, K. M.; Schinn, S.-M.; Long, E. A.; Bundy, B. C. The Emerging Impact of Cell-Free Chemical Biosynthesis. *Curr. Opin. Biotechnol.* **2018**, *53*, 115–121. https://doi.org/10.1016/j.copbio.2017.12.019.

(9) Schmid-Dannert, C.; López-Gallego, F. Advances and Opportunities for the Design of Self-Sufficient and Spatially Organized Cell-Free Biocatalytic Systems. *Curr. Opin. Chem. Biol.* **2019**, *49*, 97–104. https://doi.org/10.1016/j.cbpa.2018.11.021.

(10) Polka, J. K.; Hays, S. G.; Silver, P. A. Building Spatial Synthetic Biology with Compartments, Scaffolds, and Communities. *Cold Spring Harb. Perspect. Biol.* **2016**, *8* (8), a024018. https://doi.org/10.1101/cshperspect.a024018.

(11) Colberg, J.; Kuok (Mimi) Hii, K.; Koenig, S. G. Importance of Green and Sustainable Chemistry in the Chemical Industry. *Org. Process Res. Dev.* **2022**, *26* (8), 2176–2178. https://doi.org/10.1021/acs.oprd.2c00171.

(12) Zeymer, C.; Hilvert, D. Directed Evolution of Protein Catalysts. *Annu. Rev. Biochem.* **2018**, *87* (1), 131–157. https://doi.org/10.1146/annurev-biochem-062917-012034.

(13) *Polyelectrolyte Complexes: Fluid or Solid? | ACS Central Science*. https://pubs.acs.org/doi/10.1021/acscentsci.8b00284 (accessed 2023-04-09).

(14) Liu, Y.; Momani, B.; Winter, H. H.; Perry, S. L. Rheological Characterization of Liquid-to-Solid Transitions in Bulk Polyelectrolyte Complexes. *Soft Matter* **2017**, *13* (40), 7332–7340. https://doi.org/10.1039/C7SM01285C.

(15) *The Polyelectrolyte Complex/Coacervate Continuum | Macromolecules*. https://pubs.acs.org/doi/10.1021/ma500500q (accessed 2023-04-09).

(16) Marciel, A. B.; Chung, E. J.; Brettmann, B. K.; Leon, L. Bulk and Nanoscale Polypeptide Based Polyelectrolyte Complexes. *Adv. Colloid Interface Sci.* **2017**, *239*, 187–198. https://doi.org/10.1016/j.cis.2016.06.012.

(17) *Complexation and coacervation of like-charged polyelectrolytes inspired by mussels | PNAS*. https://www.pnas.org/doi/full/10.1073/pnas.1521521113 (accessed 2023-04-09).
(18) *Recent progress in the science of complex coacervation - Soft Matter (RSC Publishing)*. https://pubs.rsc.org/en/content/articlelanding/2020/sm/d0sm00001a (accessed 2023-04-09).
(19) Tabandeh, S.; Leon, L. Engineering Peptide-Based Polyelectrolyte Complexes with Increased Hydrophobicity. *Molecules* **2019**, *24* (5), 868. https://doi.org/10.3390/molecules24050868.
(20) Qin, J.; Priftis, D.; Farina, R.; Perry, S. L.; Leon, L.; Whitmer, J.; Hoffmann, K.; Tirrell, M.; de Pablo, J. J. Interfacial Tension of Polyelectrolyte Complex Coacervate Phases. *ACS Macro Lett.* **2014**, *3* (6), 565–568. https://doi.org/10.1021/mz500190w.
(21) Andersson, M. P.; Bennetzen, M. V.; Klamt, A.; Stipp, S. L. S. First-Principles Prediction of Liquid/Liquid Interfacial Tension. *J. Chem. Theory Comput.* **2014**, *10* (8), 3401–3408. https://doi.org/10.1021/ct500266z.
(22) Xiao, Z.; Liu, W.; Zhu, G.; Zhou, R.; Niu, Y. A Review of the Preparation and Application of Flavour and Essential Oils Microcapsules Based on Complex Coacervation Technology. *J. Sci. Food Agric.* **2014**, *94* (8), 1482–1494. https://doi.org/10.1002/jsfa.6491.
(23) Khoonkari, M.; Sayed, J. E.; Oggioni, M.; Amirsadeghi, A.; Parisi, D.; Kruyt, F.; van Rijn, P.; Włodarczyk-Biegun, M. K.; Kamperman, M. Bioinspired Processing: Complex Coacervates as Versatile Inks for 3D Bioprinting. *Adv. Mater. n/a* (n/a), 2210769. https://doi.org/10.1002/adma.202210769.
(24) Johnson, N. R.; Wang, Y. Coacervate Delivery Systems for Proteins and Small Molecule Drugs. *Expert Opin. Drug Deliv.* **2014**, *11* (12), 1829–1832. https://doi.org/10.1517/17425247.2014.941355.
(25) Peng, Q.; Wu, Q.; Chen, J.; Wang, T.; Wu, M.; Yang, D.; Peng, X.; Liu, J.; Zhang, H.; Zeng, H. Coacervate-Based Instant and Repeatable Underwater Adhesive with Anticancer and Antibacterial Properties. *ACS Appl. Mater. Interfaces* **2021**, *13* (40), 48239–48251. https://doi.org/10.1021/acsami.1c13744.
(26) Tabandeh, S.; Lemus, C. E.; Leon, L. Deciphering the Role of π-Interactions in Polyelectrolyte Complexes Using Rationally Designed Peptides. *Polymers* **2021**, *13* (13), 2074. https://doi.org/10.3390/polym13132074.
(27) Pacalin, N. M.; Leon, L.; Tirrell, M. Directing the Phase Behavior of Polyelectrolyte Complexes Using Chiral Patterned Peptides. *Eur. Phys. J. Spec. Top.* **2016**, *225* (8), 1805–1815. https://doi.org/10.1140/epjst/e2016-60149-6.
(28) Perry, S. L.; Leon, L.; Hoffmann, K. Q.; Kade, M. J.; Priftis, D.; Black, K. A.; Wong, D.; Klein, R. A.; Pierce, C. F.; Margossian, K. O.; Whitmer, J. K.; Qin, J.; de Pablo, J. J.; Tirrell, M. Chirality-Selected Phase Behaviour in Ionic Polypeptide Complexes. *Nat. Commun.* **2015**, *6* (1), 6052. https://doi.org/10.1038/ncomms7052.
(29) Stawikowski, M.; Fields, G. B. Introduction to Peptide Synthesis. *Curr. Protoc. Protein Sci. Editor. Board John E Coligan Al* **2002**, *CHAPTER*, Unit-18.1. https://doi.org/10.1002/0471140864.ps1801s26.
(30) Huang, J.; Morin, F. J.; Laaser, J. E. Charge-Density-Dominated Phase Behavior and Viscoelasticity of Polyelectrolyte Complex Coacervates. *Macromolecules* **2019**, *52* (13), 4957–4967. https://doi.org/10.1021/acs.macromol.9b00036.

(31) Banani, S. F.; Lee, H. O.; Hyman, A. A.; Rosen, M. K. Biomolecular Condensates: Organizers of Cellular Biochemistry. *Nat. Rev. Mol. Cell Biol.* **2017**, *18* (5), 285–298. https://doi.org/10.1038/nrm.2017.7.
(32) Holehouse, A. S.; Pappu, R. V. Functional Implications of Intracellular Phase Transitions. *Biochemistry* **2018**, *57* (17), 2415–2423. https://doi.org/10.1021/acs.biochem.7b01136.
(33) Marnik, E. A.; Updike, D. L. Membraneless Organelles: P Granules in Caenorhabditis Elegans. *Traffic* **2019**, *20* (6), 373–379. https://doi.org/10.1111/tra.12644.
(34) Hansma, H. G. Better than Membranes at the Origin of Life? *Life Basel Switz.* **2017**, *7* (2), 28. https://doi.org/10.3390/life7020028.
(35) Gomes, E.; Shorter, J. The Molecular Language of Membraneless Organelles. *J. Biol. Chem.* **2019**, *294* (18), 7115–7127. https://doi.org/10.1074/jbc.TM118.001192.
(36) Alberti, S.; Gladfelter, A.; Mittag, T. Considerations and Challenges in Studying Liquid-Liquid Phase Separation and Biomolecular Condensates. *Cell* **2019**, *176* (3), 419–434. https://doi.org/10.1016/j.cell.2018.12.035.
(37) Patel, A.; Lee, H. O.; Jawerth, L.; Maharana, S.; Jahnel, M.; Hein, M. Y.; Stoynov, S.; Mahamid, J.; Saha, S.; Franzmann, T. M.; Pozniakovski, A.; Poser, I.; Maghelli, N.; Royer, L. A.; Weigert, M.; Myers, E. W.; Grill, S.; Drechsel, D.; Hyman, A. A.; Alberti, S. A Liquid-to-Solid Phase Transition of the ALS Protein FUS Accelerated by Disease Mutation. *Cell* **2015**, *162* (5), 1066–1077. https://doi.org/10.1016/j.cell.2015.07.047.
(38) van Lente, J. J.; Claessens, M. M. A. E.; Lindhoud, S. Charge-Based Separation of Proteins Using Polyelectrolyte Complexes as Models for Membraneless Organelles. *Biomacromolecules* **2019**, *20* (10), 3696–3703. https://doi.org/10.1021/acs.biomac.9b00701.
(39) Neitzel, A. E.; Fang, Y. N.; Yu, B.; Rumyantsev, A. M.; de Pablo, J. J.; Tirrell, M. V. Polyelectrolyte Complex Coacervation across a Broad Range of Charge Densities. *Macromolecules* **2021**, *54* (14), 6878–6890. https://doi.org/10.1021/acs.macromol.1c00703.
(40) van Stevendaal, M. H. M. E.; Vasiukas, L.; Yewdall, N. A.; Mason, A. F.; van Hest, J. C. M. Engineering of Biocompatible Coacervate-Based Synthetic Cells. *ACS Appl. Mater. Interfaces* **2021**, *13* (7), 7879–7889. https://doi.org/10.1021/acsami.0c19052.
(41) Lim, Z. W.; Ping, Y.; Miserez, A. Glucose-Responsive Peptide Coacervates with High Encapsulation Efficiency for Controlled Release of Insulin. *Bioconjug. Chem.* **2018**, *29* (7), 2176–2180. https://doi.org/10.1021/acs.bioconjchem.8b00369.
(42) Scognamiglio, V.; Staiano, M.; Rossi, M.; D'Auria, S. Protein-Based Biosensors for Diabetic Patients. *J. Fluoresc.* **2004**, *14* (5), 491–498. https://doi.org/10.1023/b:jofl.0000039337.30726.6d.
(43) Lu, T.; Liese, S.; Schoenmakers, L.; Weber, C. A.; Suzuki, H.; Huck, W. T. S.; Spruijt, E. Endocytosis of Coacervates into Liposomes. *J. Am. Chem. Soc.* **2022**, *144* (30), 13451–13455. https://doi.org/10.1021/jacs.2c04096.
(44) Mountain, G. A.; Keating, C. D. Formation of Multiphase Complex Coacervates and Partitioning of Biomolecules within Them. *Biomacromolecules* **2020**, *21* (2), 630–640. https://doi.org/10.1021/acs.biomac.9b01354.
(45) Karoui, H.; Seck, M. J.; Martin, N. Self-Programmed Enzyme Phase Separation and Multiphase Coacervate Droplet Organization. *Chem. Sci.* **2021**, *12* (8), 2794–2802. https://doi.org/10.1039/D0SC06418A.

(46) Lafontaine, D. L. J.; Riback, J. A.; Bascetin, R.; Brangwynne, C. P. The Nucleolus as a Multiphase Liquid Condensate. *Nat. Rev. Mol. Cell Biol.* **2021**, *22* (3), 165–182. https://doi.org/10.1038/s41580-020-0272-6.
(47) Testa, A.; Dindo, M.; Rebane, A. A.; Nasouri, B.; Style, R. W.; Golestanian, R.; Dufresne, E. R.; Laurino, P. Sustained Enzymatic Activity and Flow in Crowded Protein Droplets. *Nat. Commun.* **2021**, *12* (1), 6293. https://doi.org/10.1038/s41467-021-26532-0.
(48) Kornecki, J. F.; Carballares, D.; Tardioli, P. W.; Rodrigues, R. C.; Berenguer-Murcia, Á.; Alcántara, A. R.; Fernandez-Lafuente, R. Enzyme Production of D-Gluconic Acid and Glucose Oxidase: Successful Tales of Cascade Reactions. *Catal. Sci. Technol.* **2020**, *10* (17), 5740–5771. https://doi.org/10.1039/D0CY00819B.
(49) Bauer, J. A.; Zámocká, M.; Majtán, J.; Bauerová-Hlinková, V. Glucose Oxidase, an Enzyme "Ferrari": Its Structure, Function, Production and Properties in the Light of Various Industrial and Biotechnological Applications. *Biomolecules* **2022**, *12* (3), 472. https://doi.org/10.3390/biom12030472.
(50) Nunavath, H.; Banoth, C.; Talluri, V. R.; Bhukya, B. An Analysis of Horseradish Peroxidase Enzyme for Effluent Treatment. *Bioinformation* **2016**, *12* (6), 318–323. https://doi.org/10.6026/97320630012318.
(51) Zhang, Y.; Hess, H. Inhibitors in Commercially Available 2,2'-Azino-Bis(3-Ethylbenzothiazoline-6-Sulfonate) Affect Enzymatic Assays. *Anal. Chem.* **2020**, *92* (1), 1502–1510. https://doi.org/10.1021/acs.analchem.9b04751.
(52) Park, B.-W.; Ko, K.-A.; Yoon, D.-Y.; Kim, D.-S. Enzyme Activity Assay for Horseradish Peroxidase Encapsulated in Peptide Nanotubes. *Enzyme Microb. Technol.* **2012**, *51* (2), 81–85. https://doi.org/10.1016/j.enzmictec.2012.04.004.
(53) *Proximity does not contribute to activity enhancement in the glucose oxidase–horseradish peroxidase cascade | Nature Communications*. https://www.nature.com/articles/ncomms13982 (accessed 2023-04-09).
(54) Xiong, Y.; Tsitkov, S.; Hess, H.; Gang, O.; Zhang, Y. Microscale Colocalization of Cascade Enzymes Yields Activity Enhancement. *ACS Nano* **2022**, *16* (7), 10383–10391. https://doi.org/10.1021/acsnano.2c00475.
(55) Seibert, E.; Tracy, T. S. Fundamentals of Enzyme Kinetics: Michaelis-Menten and Non-Michaelis–Type (Atypical) Enzyme Kinetics. In *Enzyme Kinetics in Drug Metabolism: Fundamentals and Applications*; Nagar, S., Argikar, U. A., Tweedie, D., Eds.; Methods in Molecular Biology; Springer US: New York, NY, 2021; pp 3–27. https://doi.org/10.1007/978-1-0716-1554-6_1.
(56) Silverstein, T. P. When Both Km and Vmax Are Altered, Is the Enzyme Inhibited or Activated? *Biochem. Mol. Biol. Educ.* **2019**, *47* (4), 446–449. https://doi.org/10.1002/bmb.21235.
(57) Wang, Y.; Wang, G.; Moitessier, N.; Mittermaier, A. K. Enzyme Kinetics by Isothermal Titration Calorimetry: Allostery, Inhibition, and Dynamics. *Front. Mol. Biosci.* **2020**, *7*, 583826. https://doi.org/10.3389/fmolb.2020.583826.
(58) Dramou, P.; Tarannum, N. 3 - Molecularly Imprinted Catalysts: Synthesis and Applications. In *Molecularly Imprinted Catalysts*; Li, S., Cao, S., Piletsky, S. A., Turner, A. P. F., Eds.; Elsevier: Amsterdam, 2016; pp 35–53. https://doi.org/10.1016/B978-0-12-801301-4.00003-7.